Ultra-slow and superluminal light propagation in solids at room temperature

2004 J. Phys.: Condens. Matter 16 R1321

(http://iopscience.iop.org/0953-8984/16/46/R01)

INSTITUTE OF PHYSICS PUBLISHING JOURNAL OF PHYSICS: CONDENSED MATTER

J. Phys.: Condens. Matter **16** (2004) R1321–R1340 PII: S0953-8984(04)86146-0

TOPICAL REVIEW

Ultra-slow and superluminal light propagation in solids at room temperature

M S Bigelow[1], **N N Lepeshkin and R W Boyd**

The Institute of Optics, University of Rochester, Rochester, NY 14627, USA

E-mail: boyd@optics.rochester.edu

Received 10 September 2004
Published 5 November 2004
Online at stacks.iop.org/JPhysCM/16/R1321
doi:10.1088/0953-8984/16/46/R01

Abstract

Slow and superluminal group velocities can be observed in any material that has large normal or anomalous dispersion. While this fact has been known for more than a century, recent experiments have shown that the dispersion can be very large without dramatically deforming a pulse. As a result, the significance and nature of pulse velocity is being reevaluated. In this review, we discuss some of the current techniques used for generating ultra-slow, superluminal, and even stopped light. While ultra-slow and superluminal group velocities have been observed in complicated systems, from an applications point of view it is highly desirable to do have this done in a solid that can operate at room temperature. We describe how coherent population oscillations can produce ultra-slow and superluminal light under these conditions.

Contents

[1] Current address: The Laser and Optics Research Center, Dept. of Physics, United States Air Force Academy, Colorado Springs, CO 80840, USA.

1. Introduction

For over 100 years, the problem of how a wave travels through a dispersive material is one that has been studied in great detail [1–5]. Recent interest in this problem has been sparked by the discovery of systems that have high dispersion, yet allow a pulse to propagate relatively undistorted. In addition, these new systems have relatively low loss so the pulse dynamics are easy to observe. However, until now, all of the systems that have been developed to generate slow or fast light are fairly complicated and difficult to implement. Specifically, these experiments are done in ultra-cold or hot atomic vapours or in solids at liquid helium temperatures. They also require precisely tuned and highly stable laser systems. For real-world applications, such complicated systems are a liability. In this review, we explore better ways to produce slow and fast light—methods that work in a room-temperature solid-state material.

1.1. Phase and group velocity

It is believed that Lord Rayleigh was the first to note the difference between the phase and group velocity [1]. The phase velocity of a monochromatic wave in a dispersive medium is defined as the velocity of points of constant phase. If the complex electric field is given as

$$\begin{aligned} E(z,t) &= E_0 \mathrm{e}^{\mathrm{i}(kz-\omega t)} \\ &= E_0 \mathrm{e}^{\mathrm{i}k(z-\frac{\omega}{k}t)}, \end{aligned} \tag{1}$$

the points of constant phase will travel at a velocity

$$v_\mathrm{p} = \frac{\omega}{k}, \tag{2}$$

where k is the wavenumber and ω is the angular frequency. This thought is frequently expressed in terms of a refractive index n_0, where $v_\mathrm{p} = c/n_0$.

If the field is not monochromatic, another velocity associated with wave propagation becomes relevant. This velocity, the group velocity, is defined as

$$v_\mathrm{g} = \frac{\mathrm{d}\omega}{\mathrm{d}k}. \tag{3}$$

In a vacuum, the group velocity is equal to the phase velocity (see figure 1) since all frequency components travel at the same speed (c). However, in general the group velocity will be different from the phase velocity. If the electromagnetic field interacts with the material at *any* frequency the material becomes dispersive at *all* frequencies, and the group velocity no longer exactly equals the phase velocity. In fact, near an optical resonance, the group velocity can be negative (see figure 2). While usually identified with the velocity of a pulse, the group velocity can be thought of as the speed of the propagating temporal interference pattern produced by multiple spectral components. For a pulse with a central frequency ω_0, the group index is given as

$$\begin{aligned} n_\mathrm{g}(\omega_0) = \frac{c}{v_\mathrm{g}} &= c\,\frac{\mathrm{d}k}{\mathrm{d}\omega} \\ &= c\,\frac{\mathrm{d}(\omega n(\omega_0)/c)}{\mathrm{d}\omega} \\ &= n(\omega_0) + \omega_0\,\frac{\mathrm{d}n(\omega_0)}{\mathrm{d}\omega}. \end{aligned} \tag{4}$$

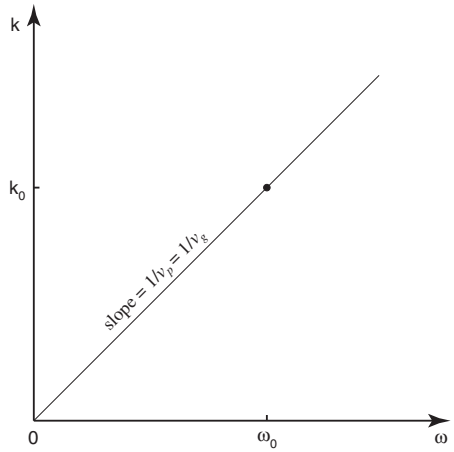

Figure 1. The dispersion diagram for electromagnetic waves travelling in a vacuum.

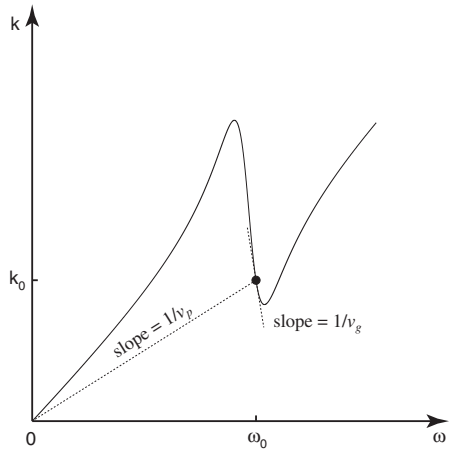

Figure 2. A dispersion curve containing a material resonance indicating the values for the phase and group velocity at a given frequency. The phase velocity is given by $v_{\mathrm{p}} = \omega_0/k_0$. The group velocity is the inverse of the slope of the dispersion curve at the frequency ω_0.

1.2. Kramers–Kronig relations

While some of the systems developed to produce large group velocities are rather exotic, they need not be. Rather, all that is necessary is to have a system where the refractive index changes rapidly as a function of frequency. This is usually done in a material which is at or near a resonance with the applied optical field. To see why this is so, we consider the Kramers–Kronig relations

$$n_{\mathrm{r}}(\omega) = 1 + \frac{c}{\pi} P \int_0^\infty \frac{\alpha(s)}{s^2 - \omega^2}\,\mathrm{d}s, \tag{5a}$$

$$\alpha(\omega) = -\frac{4\omega^2}{\pi c} P \int_0^\infty \frac{n_{\mathrm{r}}(s) - 1}{s^2 - \omega^2}\,\mathrm{d}s, \tag{5b}$$

which relate the real part of the refractive index to the absorption within the material. From a simple analysis of these equations, one can show that a narrow dip in an absorption spectrum

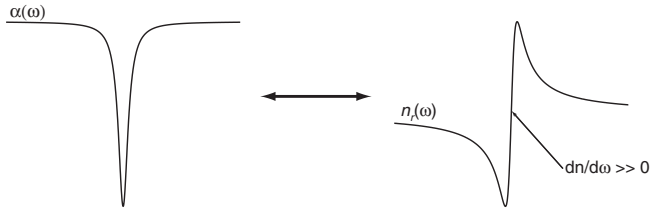

Figure 3. The absorption and refractive index are related through the Kramers–Kronig relations. A narrow spectral hole will produce strong normal dispersion.

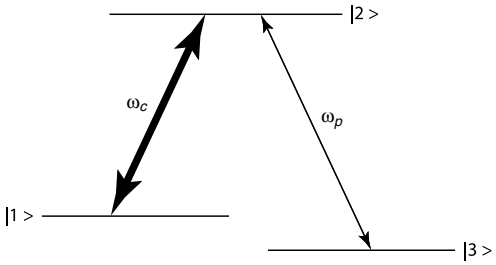

Figure 4. To produce EIT, a strong control beam (ω_p) is applied between levels $|1\rangle$ and $|2\rangle$. This effectively splits level $|2\rangle$ so that a probe beam sees reduced absorption over a very narrow spectral range.

will produce strong normal dispersion ($dn/d\omega \gg 0$), whereas a peak or gain will produce anomalous dispersion ($dn/d\omega \ll 0$). We illustrate the former case in figure 3. Since the group index of a pulse is given in equation (4) as $n_g = n_0 + \omega \frac{dn}{d\omega}$, if the dispersion is large, the group index can also be large (either positive or negative).

Therefore, the key to producing a slow (or fast) light material is to find some physical process which has a strong, but narrow spectral feature. Such a feature, by the Kramers–Kronig relations, will produce the large dispersion necessary for slow or fast light.

1.3. Ultra-slow light

It has long been known that a rapid change in the refractive index near a material resonance leads to a large value of the group index [2, 5, 6]. However, in these situations strong absorption accompanies the low group velocity making the experimental observation of these effects difficult although not altogether impossible. In the first experimental observation of slow and fast light propagation in a resonant system [7], laser pulses propagated without appreciable shape distortion, but experienced very strong resonant absorption ($\sim 10^5$ cm^{-1}).

1.3.1. EIT techniques. To reduce absorption, most of the recent work on slow light propagation has made use of the technique of electromagnetically induced transparency (EIT) to render the material medium highly transparent (see figure 4) while still retaining the strong dispersion required for the creation of slow light [8–11]. These spectral features can be so narrow that pulses are considered to be 'ultra-slow'. Using this technique, Kasapi *et al* [12] observed a group velocity of $v_g = c/165$ in a 10 cm Pb vapour cell.

Interest in this field really exploded when Hau *et al* [13] observed a group velocity of 17 m s^{-1} in a Bose–Einstein condensate (BEC). However, it has since been shown that ultra-slow group velocities are possible in more traditional states of matter. Kash *et al* [14] also used

an EIT technique to measure a group velocity of 90 m s^{-1} in a hot rubidium vapour. Using similar techniques, Budker *et al* [15] have inferred group velocities as low as 8 m s^{-1}.

In the first demonstration of ultra-slow light in a solid, Turukhin *et al* [16] have observed a velocity of 45 m s^{-1} in a praseodymium doped Y_2SiO_5 crystal. They again used EIT techniques, but in order to maintain ground state coherence, the sample had to be cooled to a cryogenic temperature of 5 K.

A classical analogue of EIT in optical oscillators has been proposed recently [17]. It was predicted that destructive interference of fields in classical coupled optical oscillators could lead to a sharp spike in transmission on resonance. This effect is very similar in appearance to the cancellation of absorption in EIT and it could lead to ultra-slow light propagation in classical optical systems at room temperature.

1.3.2. Coherent population oscillations. More recently, we demonstrated ultra-slow light for the first time in a room-temperature solid using coherent population oscillations (CPO) [18]. In the bulk of this review we will investigate this technique in detail.

1.3.3. Other techniques. Besides CPO, the only other demonstration of ultra-slow light propagation in a room-temperature solid has been the work of Podivilov *et al* [19], who slowed very long pulses to a group velocity of 0.025 cm s^{-1}. However, they observed that, in this system, the transmitted pulse experiences significant pulse distortion.

1.4. Stopped light

It has also been demonstrated that it is possible to stop or store a pulse of light and then 'release' it at a significantly later time [20–22]. Such devices could have applications in optical memories and optical computing. A dynamically controlled photonic band gas is one particularly promising technique developed by Bajcsy *et al* [22]. The key feature of this technique consists of two counter-propagating lasers that are tuned to the control field frequency in an EIT system to form periodic regions where a probe field will see reduced absorption. With only one control field present, the pulse enters the material. The second field is then applied which 'traps' the probe inside the photonic lattice. It can then be released again by turning off one of the control fields. The intriguing part of this technique is that the photonic component of the pulse never disappears; it is truly a case of stopped light.

1.5. Fast light

There has also been considerable experimental work in the production of fast light [23, 24]. Akulshin *et al* have observed a group velocity of $-c/23\,000$ using electromagnetically induced absorption [25]. More recently, Kim *et al* [26] used the same technique and observed a group velocity of $-c/14\,400$. Another technique is gain-assisted superluminal light propagation, which was first proposed by Steinberg and Chiao [27]. In this technique, a probe pulse is tuned between the gain lines produced by two pump beams. The probe sees less gain between these lines, and correspondingly large anomalous dispersion. Later Wang *et al* demonstrated a group velocity of $-c/310$ using this method [28]. More recently, Stenner *et al* [29] used a slightly modified version of the gain-assisted superluminal light propagation technique to produce pulse advancements that were nearly 11% of the width of the pulse ($v_g = -c/19.6$).

Another form of fast light is superluminal barrier tunnelling. The possibility that a particle may be able to tunnel through a barrier in a time independent of barrier width has been a point of controversy for many years [30–33]. Recently, Steinberg *et al* [34] measured the tunnelling

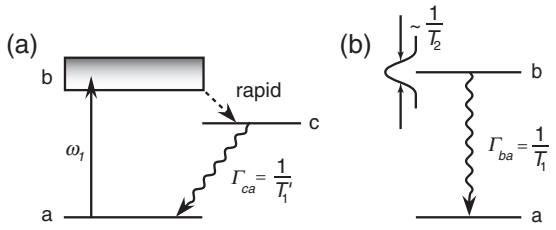

Figure 5. (a) A simplified version of the energy levels in ruby. Because of the rapid decay into level c, we can model this system as the two-level atom shown in (b).

time of a single photon through a 1D photonic band gap material and found that the photon appears on the far side of the barrier ∼1.5 fs earlier than had it been travelling in vacuum. In addition, Spielman *et al* [35] found that the pulse propagation time through a photonic band gap material is independent of the length of the material. These apparent violations of causality were resolved by Winful [36, 37], who showed that for relatively long pulses, the field of the transmitted pulse through a barrier can adiabatically follow the incident pulse with almost no delay. However, if the pulse is too narrow, the output field cannot follow the input field and no superluminal pulse advancement can be seen.

1.6. Coherent population oscillations

All of the techniques for producing both fast and slow light discussed in the last section require complicated experimental setups and/or low temperatures. However, it is important in developing applications that these large group indices can be produced in a room-temperature solid. It is this feature which makes it attractive to use the 'holes' or 'anti-holes' that are formed in homogeneously broadened absorption lines as a result of coherent population oscillations.

Spectral holes due to coherent population oscillations were first predicted in 1967 by Schwartz and Tan [38] from the solution of the density matrix equations of motion, and they have been described in greater detail by subsequent authors [39–41]. In 1983, Hillman *et al* [42] observed such a spectral hole in ruby. In their experiment, they used an argon-ion laser operating at 514.5 nm to pump population from the ground state to the broad $^4F_2$ absorption band. Population decays from this level within a few picoseconds to the metastable $2\bar{A}$ and $\bar{E}$ levels and eventually returns to the ground level with a decay time T_1' of a few milliseconds. A second probe beam (or amplitude modulation sidebands) will beat with the pump and cause the electron population to oscillate between the ground and metastable level. Because the decay time is so long, this oscillation will only occur if the beat frequency (δ) between the pump and probe beams is small so that $\delta T_1 \sim 1$. When this condition is fulfilled, the pump wave can efficiently scatter off the temporally modulated ground state population into the probe wave, resulting in reduced absorption of the probe wave. The spectral hole created is centred at the laser frequency and has a width of approximately the inverse of the population relaxation time. Hillman *et al* [42] used modulation spectroscopy to observe this feature and measured its width to be 37 Hz (HWHM).

To analyse the situation in ruby mathematically, we refer to the ground state as level a, the $^4F_2$ absorption band as level b, and the levels $2\bar{A}$ and $\bar{E}$ as level c, as illustrated in figure 5(a). Because of the rapid decay of level b, it is possible to reduce this system to a two-level system shown in figure 5(b). The density matrix equations of motion for this system are given by [43]

$$\dot{\rho}_{ba} = -\left(\mathrm{i}\omega_{ba} + \frac{1}{T_2}\right)\rho_{ba} + \frac{\mathrm{i}}{\hbar}V_{ba}w, \tag{6a}$$

$$\dot{w} = -\frac{w - w^{(\mathrm{eq})}}{T_1} - \frac{2\mathrm{i}}{\hbar}\left(V_{ba}\rho_{ab} - V_{ab}\rho_{ba}\right), \tag{6b}$$

where w is the population inversion, $T_1 = 2T_1'$ is the ground state recovery time, T_1' is the lifetime of level c, T_2 is the dipole moment dephasing time, and $w^{(\mathrm{eq})}$ is the population inversion of the material in thermal equilibrium. The distinction between T_1 and T_1' has been discussed by Sargent [39]. The interaction Hamiltonian in the rotating-wave approximation is given by $V_{ba} = -\mu_{ba}(E_1\mathrm{e}^{-\mathrm{i}\omega_1 t} + E_3\mathrm{e}^{-\mathrm{i}\omega_3 t})$, where E_1 and E_3 are the pump and probe field amplitudes, respectively, μ_{ba} is the dipole matrix element, and $\omega_3 = \omega_1 + \delta$. We seek a solution to the density matrix equation that is correct to all orders in the amplitude of the strong pump field and is correct to lowest order in the amplitude of the probe field. In this order of approximation we represent the population inversion as

$$w(t) = w^{(0)} + w^{(-\delta)}\mathrm{e}^{\mathrm{i}\delta t} + w^{(\delta)}\mathrm{e}^{-\mathrm{i}\delta t}, \tag{7}$$

where $w^{(0)}$ and $w^{(\pm\delta)}$ are given in [40] as

$$w^{(0)} = \frac{\left[1 + (\omega_1 - \omega_{ba})^2 T_2^2\right] w^{(\mathrm{eq})}}{1 + (\omega_1 - \omega_{ba})^2 T_2^2 + \Omega^2 T_1 T_2}, \tag{8a}$$

$$w^{(\pm\delta)} = \frac{\gamma}{2T_1}\frac{1 \mp \mathrm{i}\delta/\beta}{\delta^2 + \beta^2}, \tag{8b}$$

where we have defined

$$\gamma = \frac{4T_2|\mu_{ab}|^2}{\hbar^2\left[1 + (\omega_1 - \omega_{ba})^2 T_2^2\right]}\left(2E_1E_3\right), \tag{9}$$

$$\beta = \frac{1}{T_1} + \frac{4T_2|\mu_{ab}|^2}{\hbar^2}\left(E_1^2\right) = \frac{1}{T_1}\left(1 + \Omega^2 T_1 T_2\right), \tag{10}$$

and the Rabi frequency

$$\Omega \equiv \frac{2|\mu_{ab}||E_1|}{\hbar} \tag{11}$$

to simplify notation. The response at the probe frequency can be represented as [40]

$$\rho_{ba}(\omega_1 + \delta) = \frac{\mu_{ba}}{\hbar}\,\frac{E_3 w^{(0)} + E_1 w^{(\delta)}}{\omega_1 - \omega_{ba} + \mathrm{i}/T_2}. \tag{12}$$

Note that the first term corresponds to the interaction of the probe wave with the static part of the population difference (i.e. saturable absorption), whereas the second term represents the scattering of the pump wave off the temporally modulated ground state population. This contribution leads to decreased absorption at the probe frequency, that is, to a spectral hole in the probe absorption profile. To demonstrate this effect, we simplify equation (12) by assuming that $\omega_1 = \omega_{ab}$, that T_2^{-1} is large compared to the Rabi frequency and to the beat frequency $\delta \equiv \omega_3 - \omega_1$, and that $w^{(\mathrm{eq})} = -1$, to find

$$\rho_{ba}(\omega_1 + \delta) = \frac{\mathrm{i}\mu_{ba}E_3T_2}{\hbar}\left(\frac{1}{1 + \Omega^2 T_1 T_2} - \Omega^2\frac{T_2}{T_1}\frac{1 + \mathrm{i}\delta/\beta}{\delta^2 + \beta^2}\right). \tag{13}$$

We can see from the above expressions that β is the linewidth of the spectral hole. Therefore, the amplitudes of the population oscillations are appreciable only for $\delta \leqslant 1/T_1$.

We can determine the linear susceptibility through use of equation (13) by means of the relation $\chi(\delta) = N\mu_{ba}\rho_{ba}(\omega_3)/E_3$ and, consequently, find expressions for the absorption and the refractive index experienced by the probe field as

$$\alpha(\delta) = \frac{\alpha_0}{1 + I_0}\left[1 - \frac{I_0\left(1 + I_0\right)}{(T_1\delta)^2 + (1 + I_0)^2}\right], \tag{14a}$$

$$n(\delta) = 1 + \frac{\alpha_0 c}{2\omega_1}\frac{I_0}{1 + I_0}\left[\frac{T_1\delta}{(T_1\delta)^2 + (1 + I_0)^2}\right], \tag{14b}$$

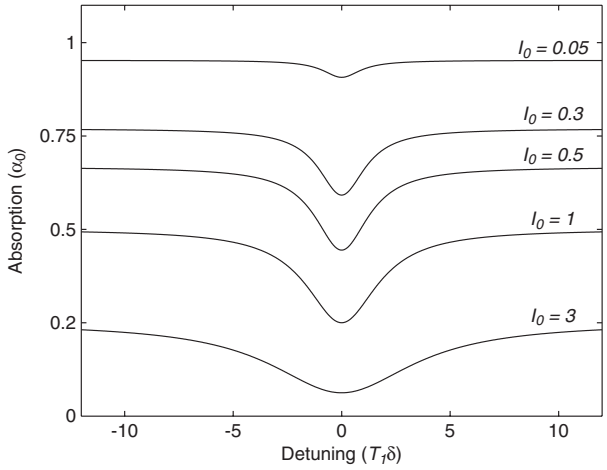

Figure 6. The absorption (in units of α_0) seen by the probe beam caused by coherent population oscillations found by plotting equation (14*a*).

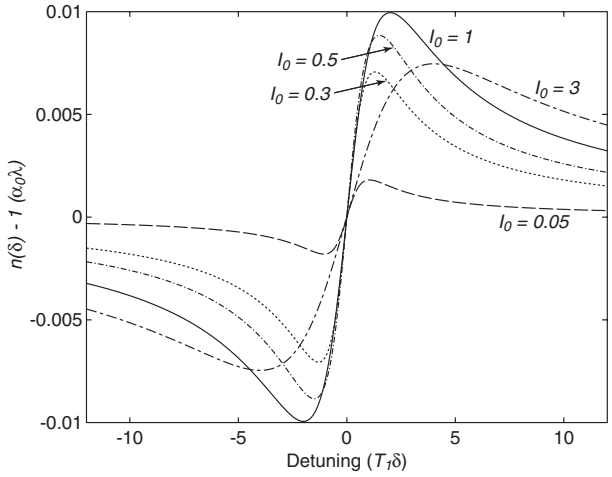

Figure 7. The refractive index change (in units of $\alpha_0\lambda$) seen by the probe beam caused by coherent population oscillations found by plotting equation (14*b*).

where $I_0 = I_1/I_{\rm sat} \equiv \Omega^2 T_1 T_2$ is the normalized pump intensity and α_0 is the unsaturated absorption coefficient.

We can plot equations (14*a*) and (14*b*) under general conditions to find how the absorption coefficient and refractive index change with pump power. In figure 6 we can see both the power-broadened spectral hole caused by coherent population oscillations and the decrease in total absorption from saturable absorption. These spectral holes correspond to rapid changes in the refractive index as a function of frequency (figure 7). We can infer from figure 7 that the dispersion is optimal when the pump intensity is equal to the saturation intensity ($I_0 = 1$). However, further analysis is necessary to verify this.

To find the group index we can rewrite equation (4) to get

$$n_g = n(\delta) + \omega_1 \frac{dn}{d\delta}. \tag{15}$$

This equation describes the propagation of spectrally narrowband pulses centred at the pump frequency ω_1. For broadband pulses, higher-order dispersion effects need to be taken into account [44]. Some of our experimental results were obtained through the use of modulation techniques such that the optical field contained only a carrier wave (to act as the pump that creates the hole) and two sidebands (to act as probes). Since this field contains discrete frequencies rather than a continuum of frequencies, a generalized form of equation (15) describing the propagation of the modulation pattern through the material is given by $n_g^{mod} = n_1 + \omega_1[n(\delta) - n(-\delta)]/2\delta$, where n_1 is the refractive index experienced by the pump. Combining this with equation (14*b*), we obtain

$$n_g^{mod} = n_1 + \frac{\alpha_0 c T_1}{2} \frac{I_0}{1+I_0} \left[\frac{1}{(1+I_0)^2 + (T_1\delta)^2} \right]. \tag{16}$$

For off-resonance modulations ($\delta \gg 1/T_1$), the modulation index reduces to $n_g^{mod} \approx n_1$. Close to resonance, the expected fractional delay of the modulation as the beam propagates a distance L is

$$\varphi^{mod} \simeq \frac{\alpha_0 L T_1}{4\pi} \frac{I_0}{1+I_0} \left[\frac{\delta}{(1+I_0)^2 + (T_1\delta)^2} \right]. \tag{17}$$

If we take the derivative of equation (17) with respect to δ and set it equal to zero, we find that the modulation frequency which has the largest fractional delay is $\delta_{max} = \beta = (1+I_0)/T_1$. Putting this result back into equation (17), we find that for a given pump intensity, the maximum possible fractional delay is

$$\varphi^{mod} = \frac{\alpha_0 L}{8\pi} \frac{I_0}{(1+I_0)^2}. \tag{18}$$

Again we can find for what values of I_0 this expression is maximum. As anticipated from figure 7, we find that φ^{mod} is largest when $I_0 = 1$. Therefore, the largest possible fractional delay due to coherent population oscillations is

$$\varphi_{max}^{mod} = \frac{\alpha_0 L}{32\pi}. \tag{19}$$

However, I_0 depends on propagation distance because of pump absorption. As a result, the optimal input intensity is somewhat above the saturation intensity. In addition, the modulation frequency where the largest effect occurs (δ_{max}) also changes with propagation distance.

Similarly, we can define a relative modulation attenuation ($A(\delta)$) as the difference between the attenuation of the modulation intensity and the attenuation of the pump intensity [39, 42] or

$$A(\delta) \equiv \ln\left[\frac{I_0(L)}{I_0(0)}\right] - \ln\left[\frac{I_{mod}(L)}{I_{mod}(0)}\right]. \tag{20}$$

To find $A(\delta)$, we know from equation (14*a*) that the modulation intensity satisfies the equation

$$\frac{dI_{mod}(z)}{dz} = -\frac{\alpha_0}{1+I_0}\left[1 - \frac{I_0(1+I_0)}{(1+I_0)^2 + (T_1\delta)^2}\right] I_{mod}(z). \tag{21}$$

Likewise, the pump intensity satisfies the equation

$$\frac{dI_0}{dz} = -\frac{\alpha_0}{1+I_0} I_0. \tag{22}$$

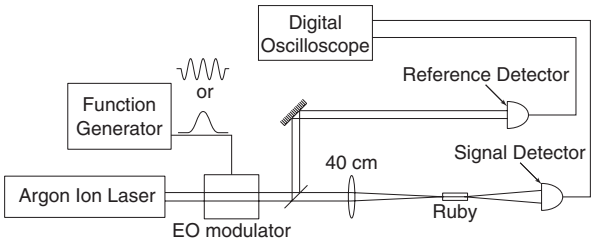

Figure 8. The experimental setup used to observe slow light in ruby.

Combining equation (22) with (21) we get

$$\frac{\mathrm{d}I_{\mathrm{mod}}}{I_{\mathrm{mod}}} = \frac{\mathrm{d}I_0}{I_0} - \frac{(1+I_0)\,\mathrm{d}I_0}{(1+I_0)^2 + (T_1\delta)^2}, \tag{23}$$

which can be exactly integrated to give

$$\ln\left[\frac{I_{\mathrm{mod}}(L)}{I_{\mathrm{mod}}(0)}\right] = \ln\left[\frac{I_0(L)}{I_0(0)}\right] - \frac{1}{2}\ln\left[\frac{(1+I_0(L))^2 + (T_1\delta)^2}{(1+I_0(0))^2 + (T_1\delta)^2}\right]. \tag{24}$$

Therefore, the relative modulation attenuation is

$$A(\delta) = \frac{1}{2}\ln\left[\frac{(1+I_0(L))^2 + (T_1\delta)^2}{(1+I_0(0))^2 + (T_1\delta)^2}\right]. \tag{25}$$

We use equations (16) and (25) in the next few sections to model the results of our experiments with ruby and alexandrite.

Up to this point, we have been treating the issue of coherent population oscillations purely in the frequency domain. However, it is useful to consider the time domain in order to understanding the delay that a pulse may experience. Consider a strong pulse that is incident on a saturable absorber. The leading edge of the pulse will experience absorption and saturate the material. Consequently, the back of the pulse will see reduced absorption with the net result being that the reshaped pulse is shifted backwards in time. Therefore, slow light due to coherent population oscillations may be equivalent to the Basov effect [45].

2. Slow light in ruby

We can utilize the results of the previous section to explicitly consider the effects of coherent population oscillations in ruby. In essence, we have repeated the work of Hillman *et al* [42], but have extended their work to include the time domain.

Our experimental setup is shown in figure 8. We used a single-line argon-ion laser operating at 514.5 nm as the laser source. The beam passed first through a variable attenuator and then an electro-optic modulator. The modulator was driven by a function generator which allowed us to either place a 6% sinusoidal amplitude modulation on the beam or produce long ($\sim$ms) pulses with almost no background intensity. For all pulse lengths, these pulses had a peak power of 0.28 W with a background that was less than 4% of that of the peak. A glass slide sent 5% of the beam to one detector for reference. The beam was then focused with a 40 cm focal length lens to a beam waist of 84 μm near the front surface of a 7.25 cm long ruby rod. Because the centre of the beam experienced less absorption than the edges due to saturation, the beam did not expand significantly in traversing the ruby. Ruby is a uniaxial crystal, and we rotated the rod to maximize the interaction. The beam exiting the ruby was

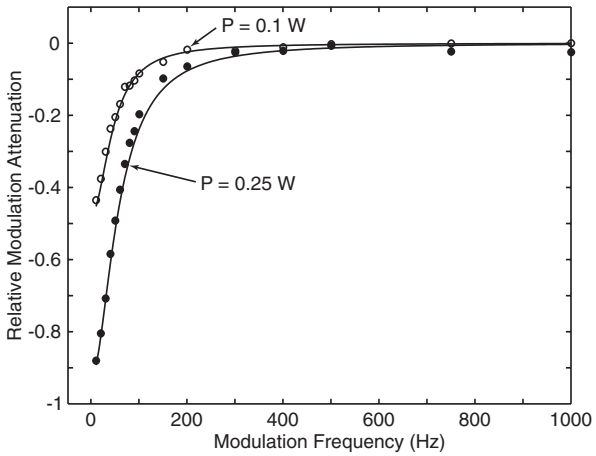

Figure 9. The relative modulation attenuation $A(\delta)$ with respect to the pump as a function of modulation frequency for input pump powers of 0.1 and 0.25 W. The solid curves represent the theoretical model of equation (25).

incident on a detector, and the detected signal was stored along with that of the input beam on a digital oscilloscope. The resulting traces were compared on a computer to calculate the relative delay and amplitude of the two signals.

To model the total group delay and modulation attenuation observed in our experiments, we first numerically calculated the value of I_0 throughout the length of the crystal. As discussed in the last section, the pump beam intensity depends on the propagation distance through the ruby as

$$\frac{\mathrm{d}I_0(z)}{\mathrm{d}z} = -\frac{\alpha_0}{1+I_0} I_0. \tag{26}$$

Using the accepted value of 1.5 kW cm^{-2} [46] for the saturation intensity of ruby at 514.5 nm, we integrated equation (26) numerically to find $I_0(z)$. Combining this function with our theoretical model for the dispersion (equations (16) and (25)), we could fit the total delay and the relative modulation attenuation measured in our experiment. We assumed α_0 and T_1 to be free parameters and found the values of $\alpha_0 = 1.17$ cm^{-1} and $T_1 = 4.45$ ms. These values are in the range found by Cronemeyer [47] and others. The total transmission in our experiments was on the order of 0.1%.

In figure 9, we show the measured relative modulation attenuation and compare it with the numerical solution of equation (25). In the limit in which the pump field becomes very weak, the spectral hole has a width of $1/(T_1 2\pi)$ or about 35.8 Hz (HWHM). As the input power is increased, the hole experiences power broadening. This result is in good agreement with the characteristics of the spectral hole that Hillman *et al* [42] found in a 1 cm ruby crystal.

This spectral dip causes an amplitude modulated beam to experience a large group index. We show the delay experienced by the modulation in figure 10 for input pump powers of 0.1 and 0.25 W. We observed the largest delay, 1.26 ± 0.01 ms, with an input pump power of 0.25 W, which corresponds in figure 9 to the power where the spectral hole is deepest but still very narrow. The inferred group velocity at this power is 57.5 ± 0.5 m s^{-1}. Note that the group velocity can be controlled by changing the modulation frequency or the input intensity. We found the nature of the effect to be strongly intensity dependent in that by moving the ruby crystal a small distance from the focus we could greatly decrease the measured delay. As a

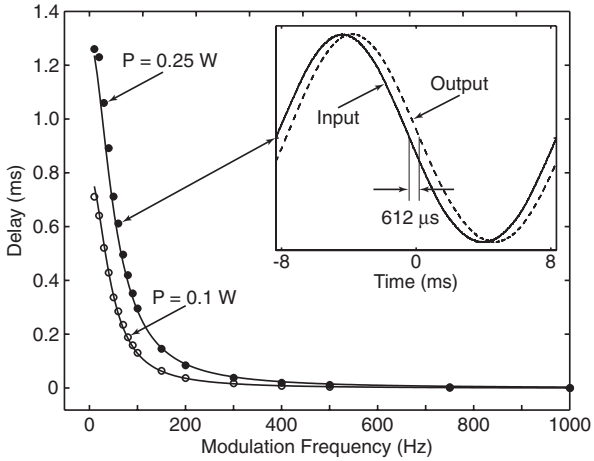

Figure 10. Observed time delay as a function of the modulation frequency for input pump powers of 0.1 and 0.25 W. The inset shows the normalized 60 Hz input (solid curve) and output (dashed curve) signal at 0.25 W. The 60 Hz signal was delayed 612 μs corresponding to an average group velocity of 118 m s^{-1}.

check of the results, we found that the time delay would completely disappear if we moved the ruby crystal far from the focus. Note that the modulation frequency with the largest fractional delay was $1/(\pi T_1) \sim 60$ Hz as we would expect. Also, the fractional delay at this frequency (3.7%) was comparable to what we would expect from equation (19).

Moreover, we have found that it was not necessary to apply separate pump and probe waves to the ruby crystal in order to observe slow light effects. A single intense pulse of light was able to provide the saturation required to modify the group index to provide slow light propagation. These relatively intense pulses can be thought of as producing their own pump field and are thus self-delayed. We know of no other examples where a separate pump beam is not required for generating ultra-slow light. For this experiment, we used the programmable pulse generator to produce Gaussian pulses with a $1/e$ intensity full width of 1–30 ms with almost no background, and we observed how they were delayed in propagating through the ruby. We found that the longer pulses also had the longer delays with the centre of mass of a 30 ms pulse delayed by 0.71 ms with little pulse distortion. We show this result and those for other pulse lengths in figure 11. While the theory developed in the last section, which assumed the presence of distinct CW pump and probe fields, does not model this pulsed experiment directly, that theory can be used to gain some intuition regarding the experiment. For instance, we would expect longer pulses, which contain lower frequency components, to experience longer delays. In addition, very short pulses with high frequency components would be expected to travel through the ruby with very little delay. As can be seen in figure 11, this insight is correct.

3. Fast light in alexandrite

Whereas a spectral hole from coherent population oscillations in a homogeneously broadened absorption line can cause slow light, an 'anti-hole' should cause fast light. Such an anti-hole with a measured width of 612 Hz was observed by Malcuit *et al* in alexandrite at 457 nm [48]. This 'anti-hole' forms instead of a hole since alexandrite is inversely saturable from roughly

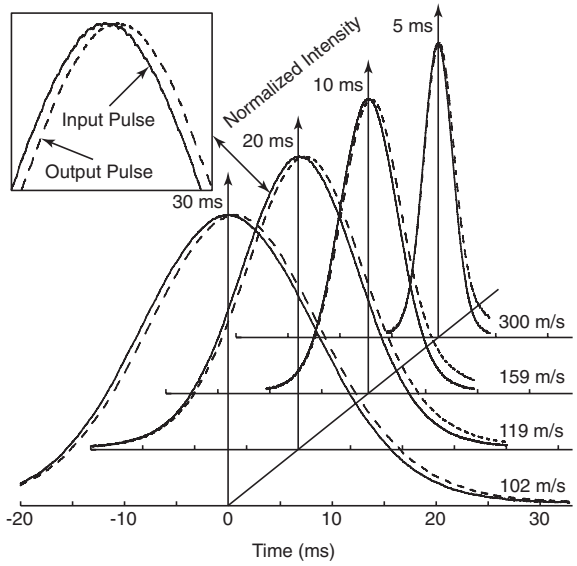

Figure 11. The normalized input and output intensities of a 5, 10, 20, and 30 ms pulse. The corresponding average group velocities of the pulses are 300, 159, 119, and 102 m s^{-1}. The inset shows a close-up of the 20 ms pulse.

450 to 510 nm due to excited state absorption [49]. However an anti-hole is not the only feature that can be seen within that wavelength range. Alexandrite is formed by doping a $BeAl_2O_4$ crystal with Cr^{3+} ions, and these ions replace the Al^{3+} ions [50]. However, not all of the ion sites are identical. Namely, 78% of the sites occupied by the Cr^{3+} ions have mirror symmetry (C_s), and the rest have inversion symmetry (C_i) [51]. As a result, the ground-state absorption cross sections σ_1, population relaxation times T_1, and the saturation intensities $I_s \equiv \frac{\hbar\omega}{\sigma_1 T_1}$ are different at each site (see figure 12). Ions at mirror sites have a relaxation time of 290 μs, and ions at inversion sites have a relaxation time of ∼50 ms [51]. The measurements suggest that the mirror-site ions have a large excited-state absorption cross section σ_2, whereas the inversion-site ions experience negligible excited-state absorption. We reached this conclusion because the width of the anti-hole (which is a consequence of excited-state absorption) is the inverse of 290 μs, whereas the width of the spectral hole (which does not involve excited-state absorption) is approximately the inverse of 50 ms. The relative size of the hole or anti-hole depends on the absorption cross sections for each site at a given wavelength.

The setup for this experiment was nearly identical to what is shown in figure 8. However this time we operated the argon-ion laser at either 457, 476, or 488 nm. Also, the beam was focused with a 20 cm focal length lens and the alexandrite crystal was 4.0 cm long. The orientation of the crystal was such that the light was polarized parallel to the *a* axis. The transmitted beam went through an interference filter to remove any signal caused by the fluorescence from electrons decaying from ^2E to the ground state and then fell onto a detector. The detected signal was stored along with that of the reference beam on a digital oscilloscope, and the resulting traces were compared on a computer to calculate the relative delay and amplitude of the two signals.

To model our results, we considered the influence of ions at both the inversion sites and the mirror sites. In addition, the absorption cross sections should be different at different wavelengths. For a given wavelength and a given ion site, we can refer to equations (14) to

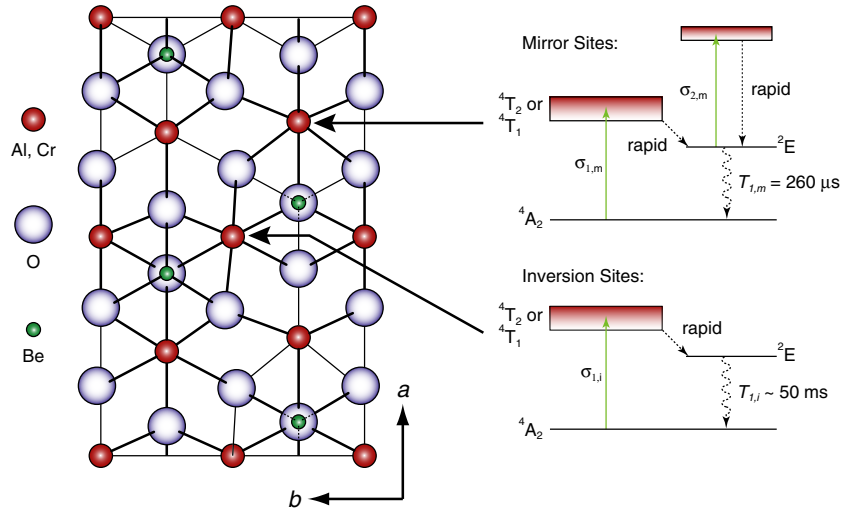

Figure 12. The crystal structure of alexandrite looking along the c axis, after [50]. The arrows indicate the locations of ion sites that have mirror or inversion symmetry. On the right are the corresponding energy-level diagrams for Cr^{3+} ions at the different sites. Mirror-site ions experience excited-state absorption and have a population relaxation time of 260 μs. Inversion-site ions have negligible excited-state absorption and a much longer population relaxation time (~50 ms).

(This figure is in colour only in the electronic version)

find the refractive index and probe beam absorption as functions of the probe beam detuning δ,

$$n(\delta) = 1 + \frac{\alpha_0 c}{2\omega_1}\frac{I_0}{1+I_0}\left[\frac{\delta T_1}{(T_1\delta)^2 + (1+I_0)^2}\right],$$
$$\alpha(\delta) = \frac{\alpha_0}{1+I_0}\left[1 - \frac{I_0\,(1+I_0)}{(T_1\delta)^2 + (1+I_0)^2}\right].$$

Since the mirror-site ions experience excited-state absorption, we can replace the unsaturated absorption coefficient α_0 for these sites with $N(\sigma_1 - \sigma_2)$, where N is the ion density. Also, we assume that the inversion-site ions experience negligible excited-state absorption and have a different saturation intensity than mirror-site ions. Now we can modify equations (14) by including a term from both the mirror sites and the inversion sites to get

$$n(\delta) = 1 + \frac{Nc}{2\omega_1}\left[\rho_m(\sigma_{1,m} - \sigma_{2,m})\frac{I_{0,m}}{1+I_{0,m}}\left(\frac{T_{1,m}\delta}{\left(T_{1,m}\delta\right)^2 + \left(1+I_{0,m}\right)^2}\right)\right.$$
$$\left. + \;\rho_i\sigma_{1,i}\frac{I_{0,i}}{1+I_{0,i}}\left(\frac{T_{1,i}\delta}{\left(T_{1,i}\delta\right)^2 + \left(1+I_{0,i}\right)^2}\right)\right], \tag{27}$$

$$\alpha(\delta) = \frac{\rho_m N(\sigma_{1,m} - \sigma_{2,m})}{1+I_{0,m}}\left[1 - \frac{I_{0,m}(1+I_{0,m})}{\left(T_{1,m}\delta\right)^2 + \left(1+I_{0,m}\right)^2}\right] + \rho_m N\sigma_{2,m}$$
$$+ \frac{\rho_i N\sigma_{1,i}}{1+I_{0,i}}\left[1 - \frac{I_{0,i}(1+I_{0,i})}{\left(T_{1,i}\delta\right)^2 + \left(1+I_{0,i}\right)^2}\right], \tag{28}$$

where the subscripts m or i indicate the parameter for the mirror or inversion sites and ρ is the percentage of ions at a given site. As we did for ruby, we calculated numerically the intensity

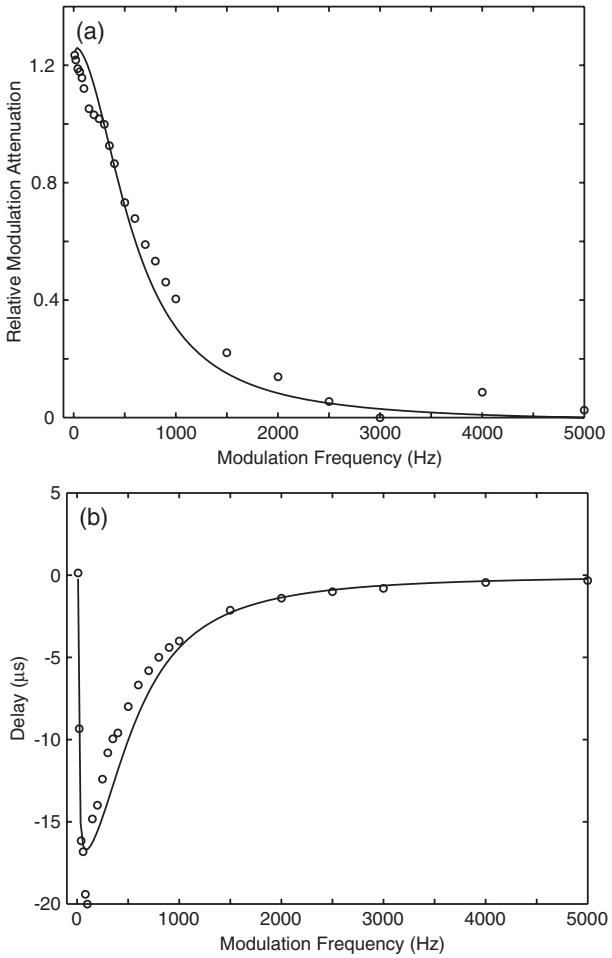

Figure 13. (a) The relative modulation attenuation and (b) the delay found in a 4 cm alexandrite crystal at a wavelength of 457 nm with a pump power of 320 mW. The observed negative time delay corresponds to superluminal propagation. The solid curves indicate the results of the theoretical model.

throughout the crystal and used these equations to find the expected delay and attenuation of the modulated signal. We found the best fit for the data using the parameters $N = 9 \times 10^{19}$ cm^{-3}, $T_{1,m} = 280$ μs, and $T_{1,i} = 19$ ms. We give the absorption cross sections that we used for each wavelength below. All of these parameters are within the range of accepted values [49, 51]. This work has been published in *Science* [52].

We independently measured the probe absorption and modulation delay as functions of frequency, and then displayed both of them to demonstrate the self-consistency of the experimental data. These results are summarized in figures 13–15. In figure 13, we show the relative modulation attenuation (as defined in section 2) and the modulation delay for a pump power of 320 mW at a wavelength of 457 nm. This is the original wavelength used by Malcuit *et al* [48]. At this wavelength, the absorption is almost completely dominated by the mirror sites. As a result, the modulation attenuation that we saw is comparable to what was observed by Malcuit *et al*. However, there is possibly some small influence of the inversion

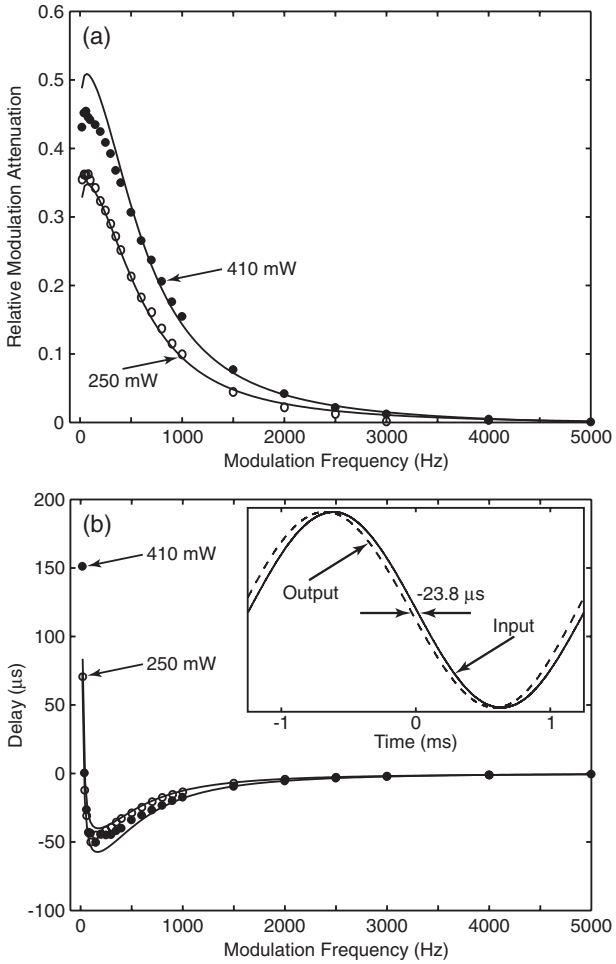

Figure 14. (a) The relative modulation attenuation and (b) the delay found in a 4 cm alexandrite crystal at a wavelength of 476 nm with a pump power of 250 and 410 mW. The solid curve indicates the results of the theoretical model. The inset in (b) shows the normalized output signal at 800 Hz leading the input signal by 23.8 μs.

sites observable primarily in the negative delay almost going to zero. In the modelling of these results, we used the values $\sigma_{1,i} = 0.1 \times 10^{-20}$ cm^2, $\sigma_{1,m} = 2.8 \times 10^{-20}$ cm^2, and $\sigma_{2,m} = 4.9 \times 10^{-20}$ cm^2. We noted that the beam transmission at this wavelength was small (<0.1%), which motivated us to look at the other laser lines of the argon-ion laser.

In figure 14, we again show the relative modulation attenuation and the accompanying delay, only this time at 476 nm and at two different pump power levels. At this wavelength, the inversion sites play a much larger role, and their influence is observable both in the small narrow dip in the relative modulation attenuation and in the corresponding positive delay at low modulation frequencies. This effect is in good agreement with the work of Schepler [53], who found that the inversion site contribution to the fluorescence intensity becomes significant from about 470–520 nm. We observed an advancement of the waveform as large as 50 μs, which corresponds to a group velocity of -800 m s^{-1} and a group index of -3.75×10^5. The measured transmission was about 3.5%. In the modelling of these results, we used the values

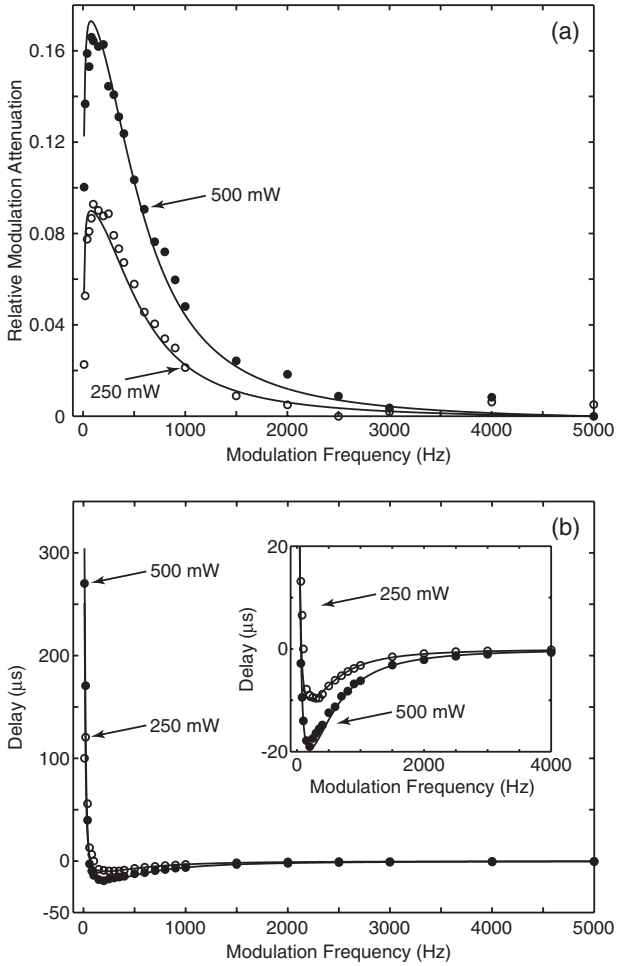

Figure 15. (a) The relative modulation attenuation and (b) the delay found in a 4 cm alexandrite crystal at a wavelength of 488 nm with a pump power of 250 and 500 mW. The solid curve indicates the results of the theoretical model. Note that ultra-slow propagation occurs for low modulation frequencies (<60 Hz), and that superluminal propagation occurs at higher frequencies. The inset in (b) is a close-up of the same data.

$\sigma_{1,i} = 0.35 \times 10^{-20}$ cm^2, $\sigma_{1,m} = 0.9 \times 10^{-20}$ cm^2, and $\sigma_{2,m} = 4.05 \times 10^{-20}$ cm^2. Using these numbers we found reasonably good agreement with the experimental data.

Finally, in figure 15 we show the same data at a wavelength of 488 nm. At this wavelength the effect of the inversion sites dominates, and produces a very narrow dip in the absorption at low frequencies. The peak in the delay shown in figure 15 corresponds to an average group velocity of 148 m s^{-1}, but we also observed group velocities as low as 91 m s^{-1} with a higher pump power (950 mW). The transmission at this wavelength was more than 10%. As can be seen from the inset in figure 15(b), we have excellent agreement with our numerical model at this wavelength using the parameters $\sigma_{1,i} = 0.4 \times 10^{-20}$ cm^2, $\sigma_{1,m} = 0.9 \times 10^{-20}$ cm^2, and $\sigma_{2,m} = 3.5 \times 10^{-20}$ cm^2.

These experiments show that it is possible to advance an amplitude modulated signal. We found that is was also possible to advance a pulse. To do this, we adjusted the electro-optic

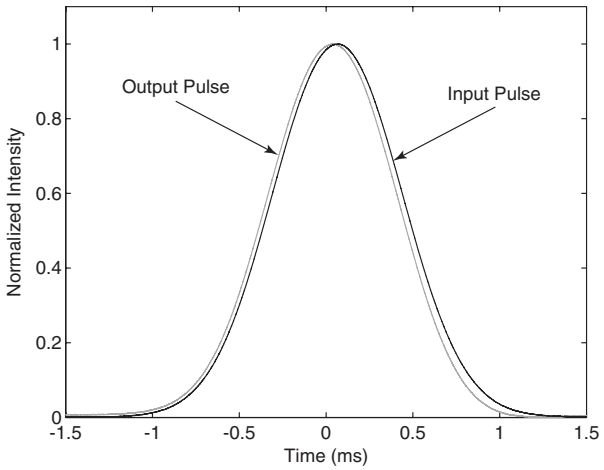

Figure 16. The input (black) and output (grey) signal for a 1 ms pulse at 476 nm. The output is advanced by 43 μs.

modulator to produce a pulse on a CW beam. The average power was 330 mW and the pulse had a peak that was 16% of the background power. The laser was tuned to the 476 nm line because the largest advancement was observed at that wavelength. We found that the centre of mass of a 1 ms pulse could be advanced as much as 43 μs with very little distortion (see figure 16).

In conclusion, we have demonstrated that either ultra-slow or superluminal light propagation can be achieved in the same solid-state material by changing the excitation wavelength. This phenomenon occurs as a result of coherent population oscillations between the ground and excited states in an alexandrite crystal. We find that we have to take account of the different absorption characteristics of Cr^{3+} ions in mirror or inversion sites to interpret our results.

4. Significance of ultra-slow light—all-optical signal processing

All-optical signal processing has the potential to revolutionize optical communication systems. For example, the cost and power consumption of the intermediate electronic elements in optical routers and hubs could be eliminated in an all-optical system. As a result, these systems can have a larger bandwidth and signal capacity than current systems.

The key element in any all-optical system is a component that will produce a tunable optical delay to allow for data buffering. Various techniques have been previously presented to create optical delay lines including fibre delay lines, Bragg gratings, and free-space optics [54, 55]. The major limitations of these techniques include the inability to control the delay, the limited optical tuning range (if any), and the lack of repeatability. Optical buffers have previously been demonstrated using a fibre loop, optical bistability [56], and accumulated echo, for use in short-term data storage. However, a slow-light-based optical buffer will allow the creation of a smart, flexible buffer with controllable delay and therefore controllable storage time. This increased flexibility will allow the buffer to be dynamically optimized for a given optical network and will result in reduced packet loss rates and increased throughput and traffic load capabilities.

EIT and CPO are the principal techniques that have been demonstrated for realizing controllable 'slow light' and increasing the strength of nonlinear optical interactions, a promising path for addressing both of the critical issues discussed above. Slowing the group velocity of pulses will allow for delay lines with shorter physical length, and increasing the size of the nonlinear optical interaction will allow for smaller all-optical processing elements. Such advances will bring key functional elements down to the chip scale and allow a new generation of dense photonic integration platforms to be realized.

5. Summary and conclusions

In this review, we first described the concept of coherent population oscillations—the primary physical mechanism we used to generate large dispersion. We showed that when the beat frequency between the pump and probe beams is slow enough, it will cause the population in a two-level atom to oscillate. This time-varying population will cause energy to be scattered out of the pump beam and into the probe. As a result, the probe will see less absorption over a narrow frequency range. Correspondingly, the group velocity for the probe can be very large within the same frequency range. From our investigations, it is clear that coherent population oscillations are possible in a wide variety of systems.

We described our experimental demonstration of ultra-slow light propagation in ruby using coherent population oscillations. We observed a group velocity as low as 58 m s^{-1}, which is a comparable group velocity to what is observed using much more difficult EIT techniques. Our results included the observation of a delay of both amplitude modulations and pulses. Therefore, our method is validated as an important new way to generate ultra-slow group velocities.

We further extended the investigation of coherent population oscillations to a different material. In alexandrite, we showed how it is possible to observe both ultra-slow and superluminal group velocities. Since alexandrite is an inverse saturable absorber at certain wavelengths, the sign of the group velocity is changed. In addition, alexandrite has a slightly more complicated structure than ruby in that the chromium ions can occupy two different types of lattice sites within the crystal. These two types of sites are known as mirror sites (having mirror symmetry) and inversion sites (having inversion symmetry). Due to the energy level structure at each site, ions at mirror sites experience inverse-saturable absorption (fast light), whereas ions at inversion sites experience saturable absorption (slow light). The competing effects from ions at either site can be easily distinguished because they have markedly different population relaxation times.

Finally, we discussed the significance of ultra-slow light propagation. While much work remains to be done, we conclude that these slow light techniques could be very important in developing all-optical control of communication and storage applications.

Acknowledgment

This work was supported by NSF grant ECS-0355206.

References

[1] Lord Rayleigh 1877 *Proc. London Math. Soc.* **9** 21
[2] Brillouin L 1960 *Wave Propagation and Group Velocity* (New York: Academic)
[3] Smith R L 1970 *Am. J. Phys.* **38** 978
[4] Oughstun K E and Sherman G C 1994 *Electromagnetic Pulse Propagation in Causal Dielectrics* (Berlin: Springer)

[5] Boyd R W and Gauthier D J 2002 *Progress in Optics* vol 43, ed E Wolf (Amsterdam: Elsevier) pp 497–530
[6] Garrett C G B and McCumber D E 1970 *Phys. Rev.* A **1** 305
[7] Chu S and Wong S 1982 *Phys. Rev. Lett.* **48** 738
[8] Tewari S P and Agarwal G S 1986 *Phys. Rev. Lett.* **56** 1811
[9] Harris S E, Field J E and Imamoglu A 1990 *Phys. Rev. Lett.* **64** 1107
[10] Harris S E, Field J E and Kasapi A 1992 *Phys. Rev.* A **46** R29
[11] Bennink R S *et al* 2001 *Phys. Rev.* A **63** 033804
[12] Kasapi A *et al* 1995 *Phys. Rev. Lett.* **74** 2447
[13] Hau L V *et al* 1999 *Nature* **397** 594
[14] Kash M M *et al* 1999 *Phys. Rev. Lett.* **82** 5229
[15] Budker D *et al* 1999 *Phys. Rev. Lett.* **83** 1767
[16] Turukhin A V *et al* 2002 *Phys. Rev. Lett.* **88** 023602
[17] Smith D D *et al* 2004 *Phys. Rev.* A **69** 063804
[18] Bigelow M S, Lepeshkin N N and Boyd R W 2003 *Phys. Rev. Lett.* **90** 113903
[19] Podivilov E, Sturman B, Shumelyuk A and Odoulov S 2003 *Phys. Rev. Lett.* **91** 083902
[20] Liu C, Dutton Z, Behroozi C H and Hau L V 2001 *Nature* **409** 490
[21] Phillips D F *et al* 2001 *Phys. Rev. Lett.* **86** 783
[22] Bajcsy M, Zibrov A S and Lukin M D 2003 *Nature* **426** 638
[23] Ségard B and Macke B 1985 *Phys. Lett.* A **109** 213
[24] Talukder M A I, Amagishi Y and Tomita M 2001 *Phys. Rev. Lett.* **86** 3546
[25] Akulshin A M, Barreiro S and Lezema A 1999 *Phys. Rev. Lett.* **83** 4277
[26] Kim K *et al* 2003 *Phys. Rev.* A **68** 013810
[27] Steinberg A M and Chiao R Y 1994 *Phys. Rev.* A **49** 2071
[28] Wang L J, Kuzmich A and Dogariu A 2000 *Nature* **406** 277
[29] Stenner M D, Gauthier D J and Neifeld M A 2003 *Nature* **425** 695
[30] MacColl L A 1932 *Phys. Rev.* **40** 621
[31] Wigner E P 1955 *Phys. Rev.* **98** 145
[32] Hartman T E 1962 *J. Appl. Phys.* **33** 3427
[33] Chiao R Y and Steinberg A M 1997 *Progress in Optics* vol 37, ed E Wolf (Amsterdam: Elsevier) pp 345–405
[34] Steinberg A M, Kwiat P G and Chiao R Y 1993 *Phys. Rev. Lett.* **71** 708
[35] Spielmann Ch, Szipöcs R, Stingl A and Krausz F 1994 *Phys. Rev. Lett.* **73** 2308
[36] Winful H G 2003 *Phys. Rev. Lett.* **90** 023901
[37] Winful H G 2003 *Nature* **424** 638
[38] Schwartz S E and Tan T Y 1967 *Appl. Phys. Lett.* **10** 4
[39] Sargent M III 1978 *Phys. Rep.* **43** 223
[40] Boyd R W *et al* 1981 *Phys. Rev.* A **24** 411
[41] Wilson-Gordon A D 1993 *Phys. Rev.* A **48** 4639
[42] Hillman L W *et al* 1983 *Opt. Commun.* **45** 416
[43] Boyd R W 1992 *Nonlinear Optics* (San Diego, CA: Academic)
[44] Peatross J, Glasgow S A and Warr M 2000 *Phys. Rev. Lett.* **84** 2370
[45] Basov N G *et al* 1966 *Sov. Phys.—JETP* **23** 16
[46] Liao P F and Bloom D M 1978 *Opt. Lett.* **3** 4
[47] Cronemeyer D C 1966 *J. Opt. Soc. Am.* **56** 1703
[48] Malcuit M S, Boyd R W, Hillman L W, Kasinski J and Stroud C R Jr 1984 *J. Opt. Soc. Am.* B **1** 73
[49] Shand M L, Walling J C and Morris R C 1981 *J. Appl. Phys.* **52** 953
[50] Farrell E F, Fang J H and Newnham R E 1963 *Am. Mineral.* **48** 804
[51] Powell R C, Xi L, Gang X and Quarles G J 1985 *Phys. Rev.* B **32** 2788
[52] Bigelow M S, Lepeshkin N N and Boyd R W 2003 *Science* **301** 200
[53] Schepler K L 1984 *J. Appl. Phys.* **56** 1314
[54] Rader A and Anderson B L 2003 *Appl. Opt.* **42** 1409
[55] Pape D R and Goutzoulis A P 1999 *J. Opt. A: Pure Appl. Opt.* **1** 320
[56] Miller D, Smith S and Seaton C 1981 *IEEE J. Quantum Electron.* **17** 312